NATIONAL ADVISORY COMMITTEE FOR AERONAUTICS

WARTIME REPORT

ORIGINALLY ISSUED
March 1945 as
Memorandum Report L5C12c

HIGH-SPEED PHOTOGRAPHS OF A YR-4B PRODUCTION ROTOR BLADE FOR SIMULATED FLIGHT CONDITIONS IN THE LANGLEY FULL-SCALE TUNNEL

By Richard C. Dingeldein and Raymond F. Schaefer

Langley Memorial Aeronautical Laboratory
Langley Field, Va.

NACA

WASHINGTON

MR No. L5C12c

NATIONAL ADVISORY COMMITTEE FOR AERONAUTICS

MEMORANDUM REPORT

HIGH-SPEED PHOTOGRAPHS OF A YR-4B PRODUCTION ROTOR BLADE FOR SIMULATED FLIGHT CONDITIONS IN THE LANGLEY FULL-SCALE TUNNEL

By Richard C. Dingeldein and Raymond F. Schaefer

SUMMARY

Recent tests of a Sikorsky YR-4B helicopter in the Langley full-scale tunnel included photographing a production rotor blade in simulated forward-flight conditions using Edgerton flash equipment. The blade was photographed at azimuth angles of 0°, 45°, 135°, 180°, 225°, and 315° for tip-speed ratios ranging from 0.12 to 0.23.

The results clearly show fabric deformation in the form of sagging and bulging. The photographs also indicate a reversal in the bending curve near the blade tip that appears to result from the combined effects of losses of lift and high centrifugal force at this point.

INTRODUCTION

A Sikorsky YR-4B helicopter has been tested in the Langley full-scale tunnel at the request of the Army Air Forces, Air Technical Service Command. One phase of the tests consisted of taking high-speed photographs of a YR-4B production rotor blade at different azimuth angles for simulated forward-flight conditions using Edgerton flash equipment supplied and operated by personnel of the Photo Engineering Branch, Technical Data Laboratory, Engineering Division, Wright Field, Ohio. The blade photographs for the different test conditions are presented in this paper.

APPARATUS

The Sikorsky YR-4B helicopter was mounted at the three landing-gear supports on a direct-reading, six-component strain-gage balance. The strain gages were calibrated for a center of gravity located on the center line of the main rotor shaft 56.52 inches below the plane of the flapping hinges. This position was chosen from information supplied by the manufacturer and falls within the center-of-gravity range corresponding to normal gross weight. The pitch angle was obtained from an indicator attached to the control linkage and calibrated against a protractor mounted on a rotor blade at the 0.75 radius. The power input to the main rotor was measured by a strain-gage-type torquemeter located on the rotor shaft. The indicators for the pitch angle and the strain-gage balance and torquemeter, together with the remote-control system which operated the engine and flight controls of the helicopter, were located in a test house at the rear of the balance house. The general arrangement of the test setup is shown in figure 1.

A photograph of a YR-4B production blade and pertinent dimensions are shown in figure 2. These blades have a radius of 19 feet measured from the center of rotation, a tapered plan form, a total area (three blades) of 65.4 square feet, and are untwisted. The solidity based on the weighted chord is 0.060. An NACA 0012 airfoil section is used. The blade consists of a tubular steel spar to which 36 wooden ribs are attached. The ribs are spaced approximately 6 inches at the root and $4\frac{1}{2}$ inches at the tip. Spruce fairing strips contour the blade surface for the forward 35 percent of the chord. A wire cable forms the trailing edge and the entire rotor blade is fabric-covered. A single 3/16-inch-diameter vent hole is located on the lower surface of the rotor blade approximately 6 inches from the blade tip at 38 percent of the chord. (See fig. 2.)

PHOTOGRAPHIC EQUIPMENT

The special high-speed photographic equipment included two modified K-15A aerial cameras, an Edgerton flash lamp, and a portable gasoline-driven generator.

Each camera was modified to the extent of removing the shutter and the intermittent film-transport mechanism. The high-intensity flash from the Edgerton lamp was of approximately 1/10000 second duration. The lamp was discharged at a given rotor-blade azimuth angle by a micro switch which was tripped by an adjustable cam mounted on the rotor shaft. One camera and the Edgerton lamp were mounted on the base of the wind-tunnel survey carriage (see fig. 3) and set at the same elevation as the rotor hub to photograph a rotor blade in the plane of rotation. The second camera, which was fastened to the tunnel structure directly over the main-rotor shaft for a helicopter angle of attack of 0°, simultaneously recorded the azimuth position of the rotor blade. The relative location of the equipment with respect to the helicopter is shown in figure 4.

TEST CONDITIONS

The same rotor blade was photographed at four tip-speed ratios from 0.12 to 0.23 for azimuth angles of approximately 0°, 45°, 135°, 180°, 225°, and 315° for simulated level-flight conditions. An engine speed of 1800 rpm (193 rotor rpm) was used throughout the tests because of the excessive vibration of the helicopter and supports encountered at higher speeds. This condition corresponds to a Reynolds number of 2.05×10^6 at the 0.75 radius and a rotational tip speed of 384 feet per second. The gross weight of the helicopter was taken as 2500 pounds. The spindle angle for trimmed flight at each tunnel airspeed was determined from the flight-test data presented in reference 1. This angle was corrected for the tunnel jet-boundary effect by assuming the rotor disc is equivalent to a wing of the same span, area, and lift. The induced flow through the rotor materially reduced the tunnel airspeed, especially for the lower forward speeds. Due to this effect and to the changes in the tunnel stream angle caused by the rotor, the spindle settings used only approximate those for trimmed flight conditions. For this reason it was impossible to trim both the forces and moments simultaneously at a lift of 2500 pounds. The moments were considered more important and were therefore trimmed to zero. The magnitude of the unbalanced drag and side force is given for all conditions.

RESULTS AND DISCUSSION

The test conditions for which the blade pictures were obtained are listed in table I. The high-speed photographs of a rotor blade taken in the plane of rotation for the four test conditions are presented in figures 5 through 10 for the six azimuth angles. The pictures taken for condition 1 by the overhead camera for these azimuth positions are shown in figure 11. The actual azimuth angles corresponding to 0°, 45°, 135°, 180°, 225°, and 315° are shown to be 0°, 47°, 131°, 181°, 223°, and 308° and are expected to be approximately the same for conditions 2, 3, and 4, inasmuch as the blades were photographed at the same rotor-shaft cam setting for all four conditions.

The photographs of figures 5 through 10 show the type of surface deformation that occurs on a fabric-covered rotor blade. Because of the nature of the external pressures which produce rotor-blade lift, internal pressures below free-stream static pressure will exist somewhat outboard of the point at which fabric sagging appears on the upper blade surface. Similarly, internal pressures greater than free-stream static pressure will exist somewhat inboard of the point at which fabric bulging is shown on the lower surface. The spanwise distribution of internal pressure has been roughly estimated from the photographs, which indicate that the internal pressure from the root to approximately the 77-percent radius (25th rib) is below free-stream static pressure. The fabric bulging on the lower surface is difficult to detect from the photographs; however, the internal pressures for approximately the outboard 10 percent of the radius appear to be greater than free-stream static pressure. Calculations prove that the difference in internal pressure between the blade root and the tip, assuming no intermediate venting, will be equal to the dynamic pressure at the tip. This amounts to approximately 34 inches of water in the present case. The results of the tests of rotor-blade sections in two-dimensional flow published in reference 2 indicate that the bulged portions of the blade will probably cause an increase in section drag coefficient, a decrease in maximum section lift coefficient, and a forward movement of the aerodynamic center. The effect of fabric sagging is indicated by the same

source to be a slight increase in section drag coefficient, a slight increase in maximum section lift coefficient, and a slight rearward movement of the aerodynamic center. Inasmuch as higher velocities occur over the outer portions of the blades, the effects due to bulging would be expected to predominate.

The use of closer rib spacing to obtain a more uniform rotor-blade surface is suggested by the photographs, especially those of figure 11 in which the lighting accentuates the sagging over the inboard blade sections. Tests of two rotor-blade sections, one of which had half the rib spacing of the other, are reported in reference 2. The advantages of improved surface conditions are also indicated in reference 3, which compares the static-thrust performance of this same rotor blade with that of other rotor blades having a more rigid surface.

In almost all of the high-speed photographs the rotor blade droops distinctly near the tip. This effect may be the result of a loss of lift at the blade tip, together with the predominance of the centrifugal force at this point. It is not believed to be the result of inertia loads occurring during flapping since only a small part of the droop appears to be periodic.

CONCLUDING REMARKS

The high-speed photographs of a Sikorsky YR-4B production rotor blade in simulated flight conditions show the fabric sagging and bulging caused by the centrifugal force acting on the mass of air enclosed by the blade. The internal pressure is indicated to be less than the free-stream static pressure from the root to approximately the 77-percent radius and to be greater than free-stream static pressure for approximately the outboard 10 percent of the radius. There is a reversal in the bending curve near the blade tip that appears to

result from the combined effects of losses of lift and high centrifugal force at this point.

Langley Memorial Aeronautical Laboratory
National Advisory Committee for Aeronautics
Langley Field, Va.

REFERENCES

1. Gustafson, F. B.: Flight Tests of the Sikorsky HNS-1 (Army YR-4B) Helicopter. I - Experimental Data on Level-Flight Performance with Original Rotor Blades. NACA MR No. L5C10, 1945.

2. Tetervin, Neal: Airfoil Section Data from Tests of 10 Practical Construction Sections of Helicopter Rotor Blades Submitted by the Sikorsky Aircraft Division, United Aircraft Corporation. NACA MR, Sept. 6, 1944.

3. Dingeldein, Richard C., and Schaefer, Raymond F.: Static-Thrust Tests of Six Rotor-Blade Designs on a Helicopter in the Langley Full-Scale Tunnel. NACA ARR No. L5F25b, 1945.

Table I.- Wind-Tunnel Settings and Results for Test Conditions.

Item	Condition 1	2	3	4
Tip-speed ratio, μ	0.12	0.16	0.20	0.23
Tunnel spindle angle, α_T, deg	3.6	0.5	-1.9	-3.8
Corrected spindle angle, α_c, deg	-3.4	-3.6	-4.6	-6.0
Dynamic pressure, $\frac{1}{2}\rho V^2$, lb/sq ft	2.46	4.48	7.32	9.40
Tunnel airspeed, V, mph	30.9	41.6	53.2	60.2
Indicated total pitch angle at 0.75 R, θ, deg.	9.5	10.0	10.5	10.5
Lift, L, lb. *	2498	2501	2515	2502
Drag, D, lb.*	-61	4	-88	-91
Side force, Y, lb.	170	215	214	214
Main-rotor thrust coefficient, C_T	0.0062	0.0062	0.0063	0.0062
Main-rotor torque coefficient, C_Q	0.00036	0.00036	0.00041	0.00046

* Lift and drag are given for corrected wind axes.

NATIONAL ADVISORY
COMMITTEE FOR AERONAUTICS.

Symbols used are defined as follows:

μ tip-speed ratio ($V \cos\alpha / \Omega R$)
Ω rotor angular velocity, rad/sec
R rotor radius, 19 ft.
C_T rotor thrust coefficient ($T/\rho\Omega^2\pi R^4$)
T rotor thrust, lb.
C_Q rotor torque coefficient ($Q/\rho\Omega^2\pi R^5$)
Q rotor torque, ft-lb
Ψ blade azimuth angle, deg. (measured from downwind position in direction of rotation)

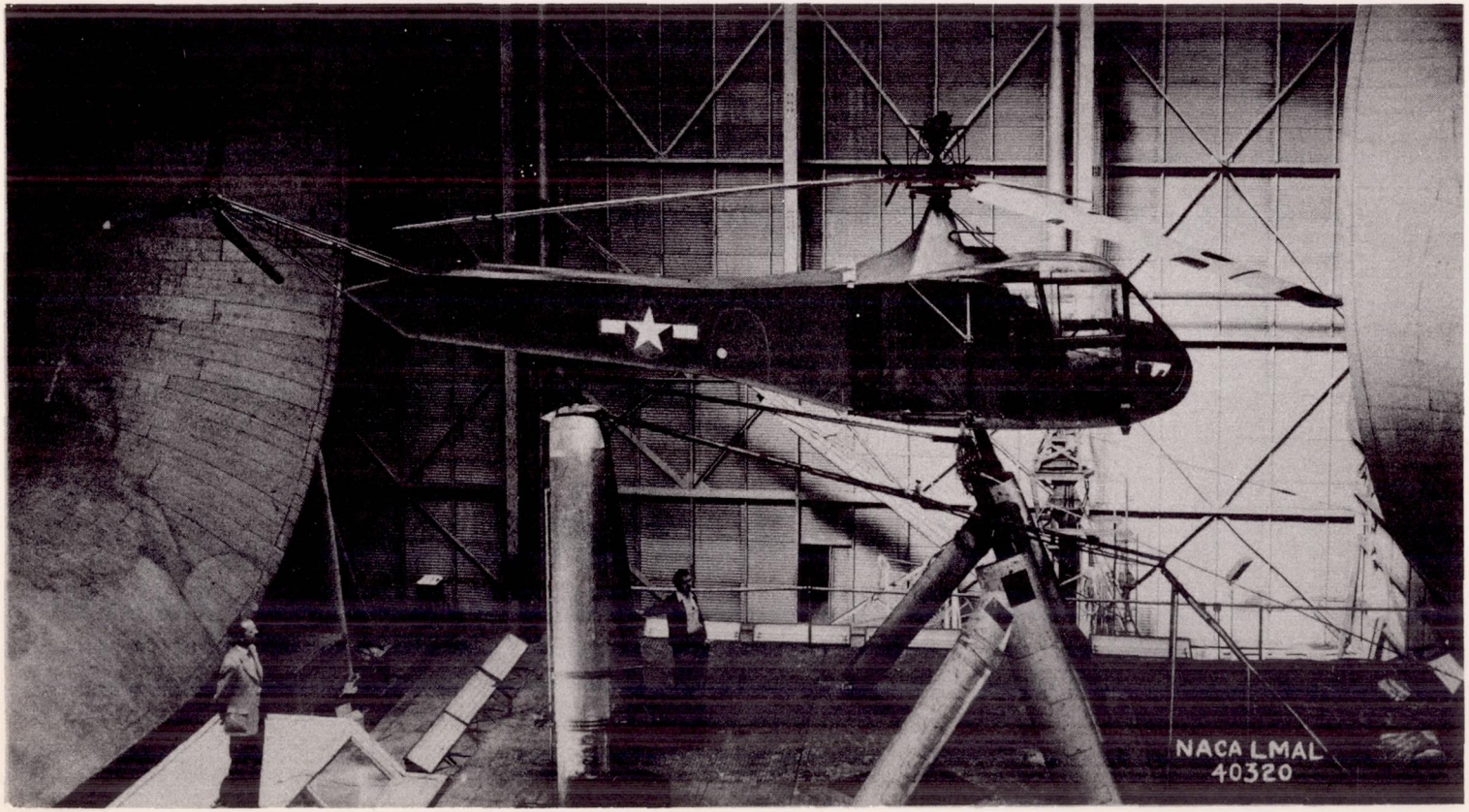

Figure 1.- The YR-4B helicopter mounted in the Langley full-scale tunnel.

MR No. L5C12c

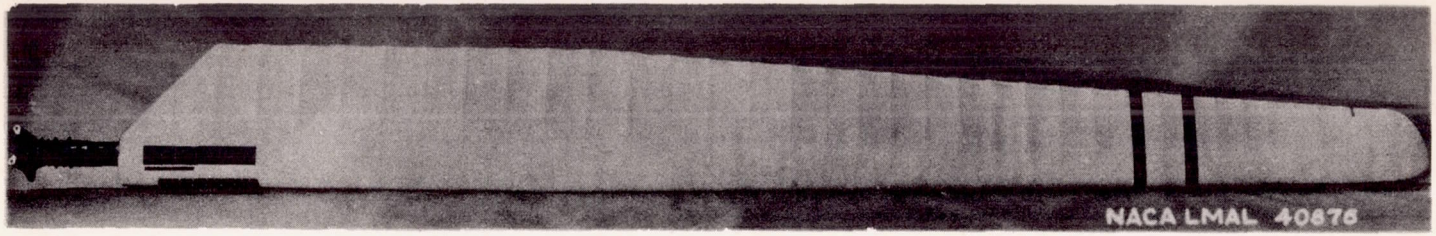

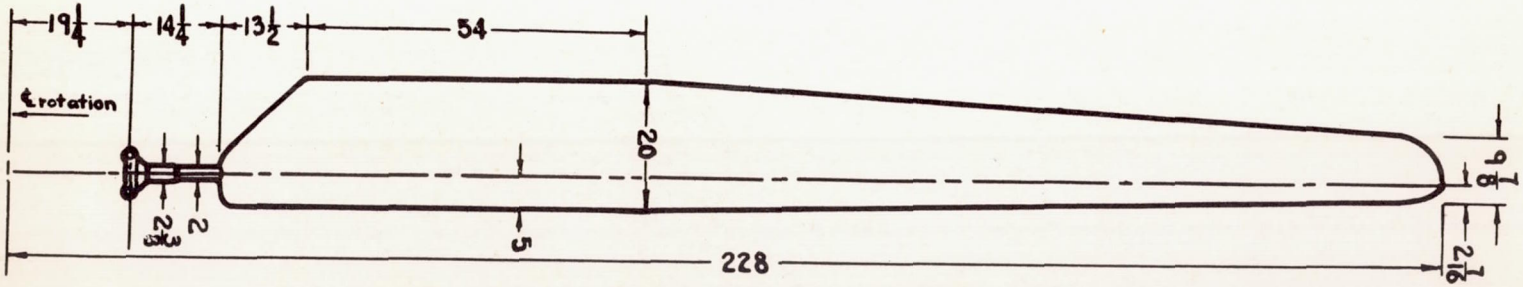

Figure 2.- YR-4B production blade. Lower surface shown. (All dimensions given in inches).

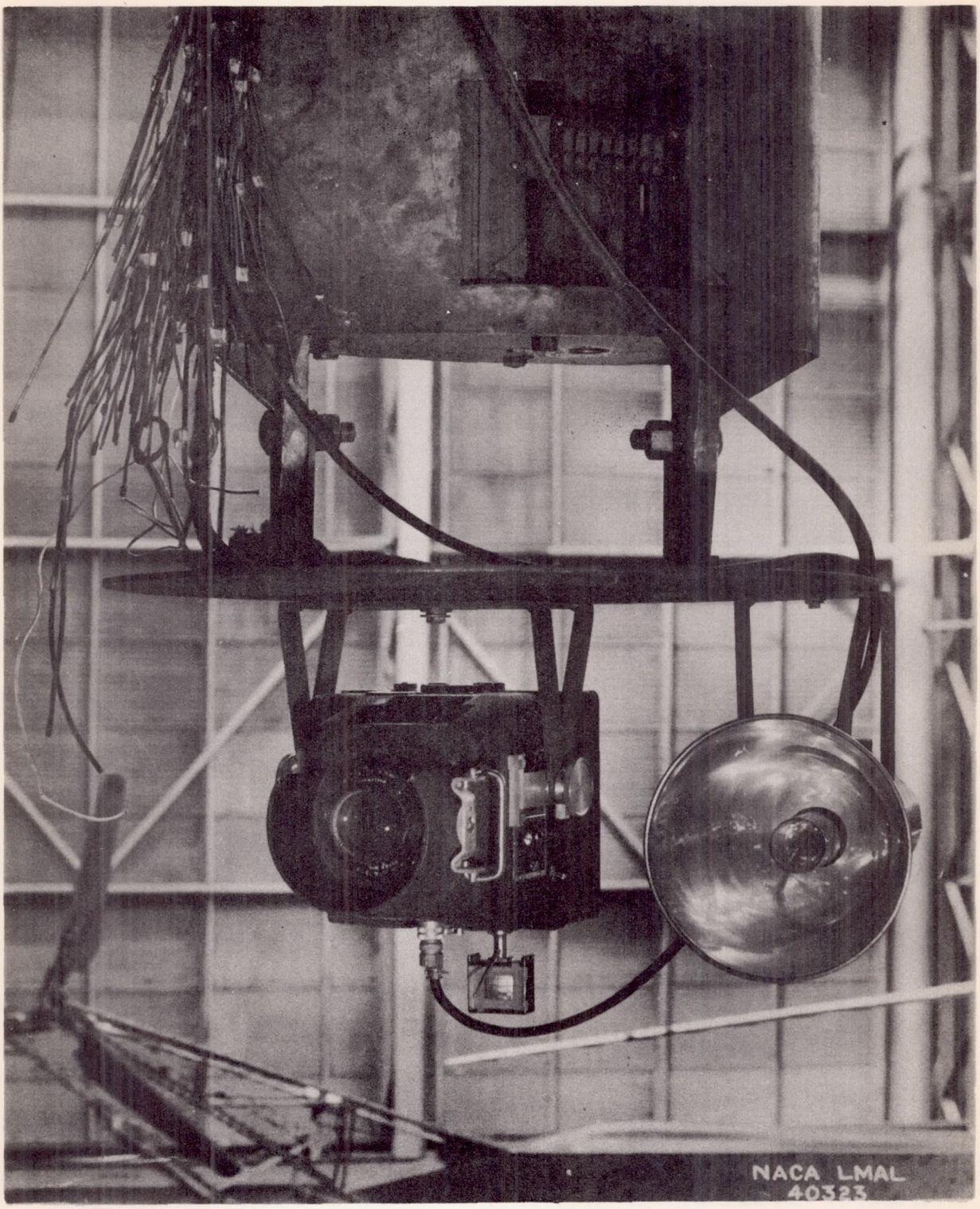

Figure 3.- Modified K-15A aerial camera and Edgerton flash lamp mounted on base of survey carriage.

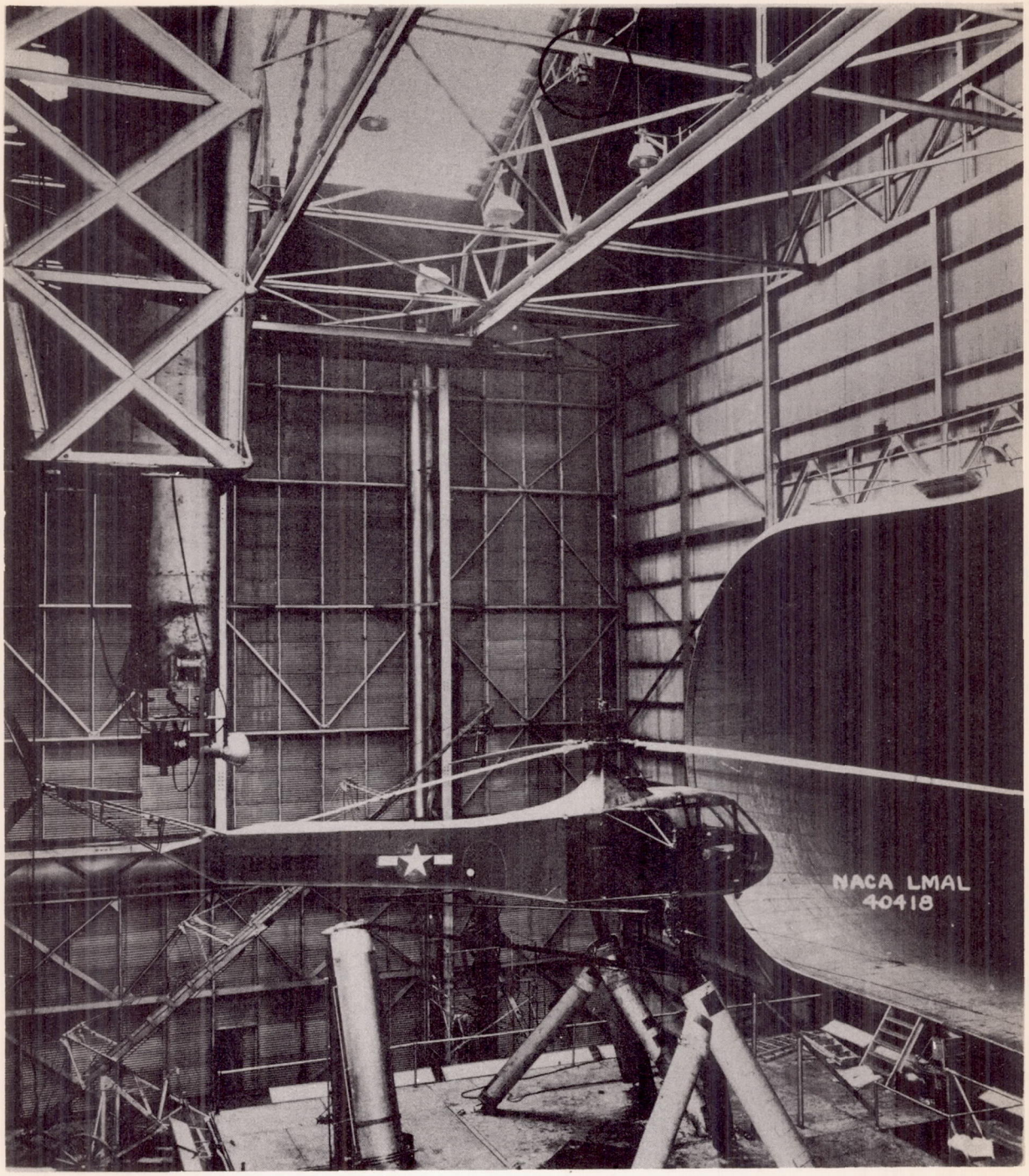

Figure 4.- General view of photographic equipment and YR-4B helicopter in the Langley full-scale tunnel.

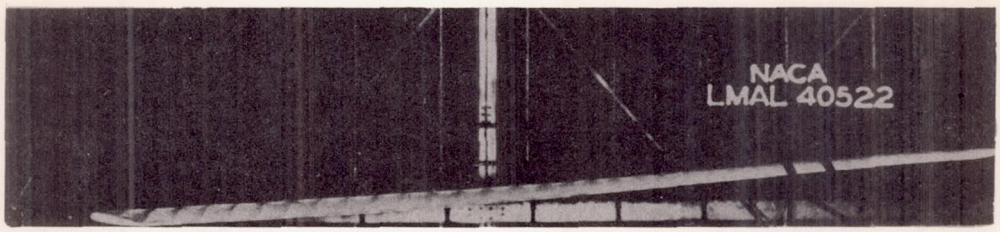

a. Condition 1.

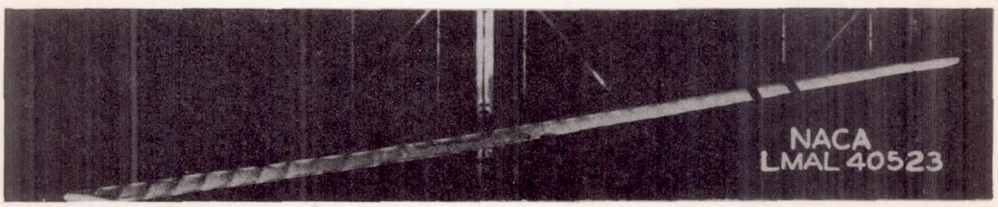

b. Condition 2.

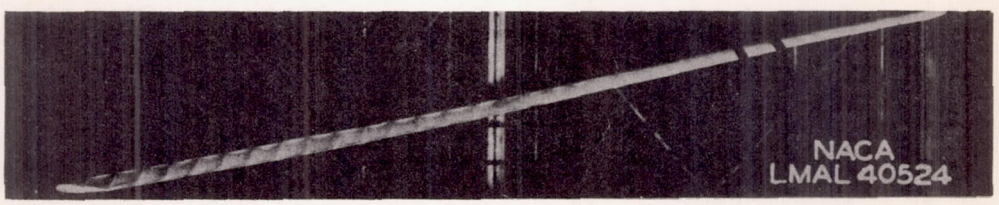

c. Condition 3.

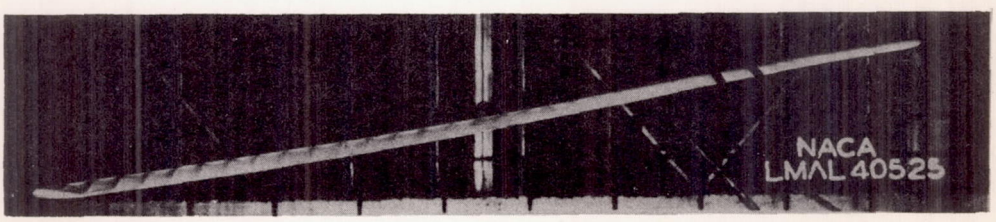

d. Condition 4.

Figure 5.- High-speed photographs of a YR-4B production rotor blade in simulated flight conditions, ψ, 0°.

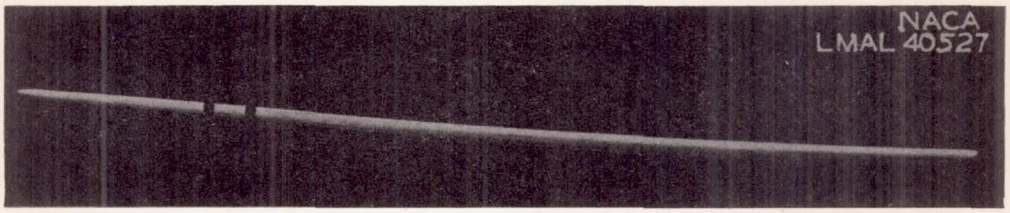

a. Condition 1

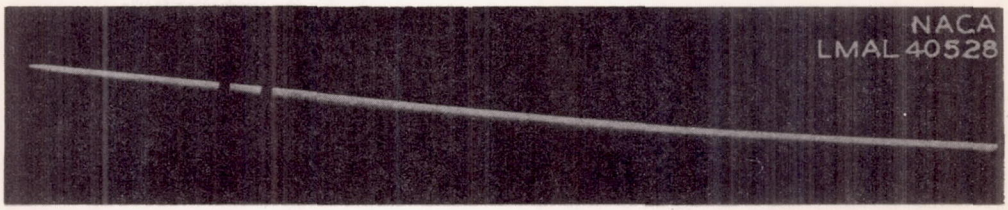

b. Condition 2.

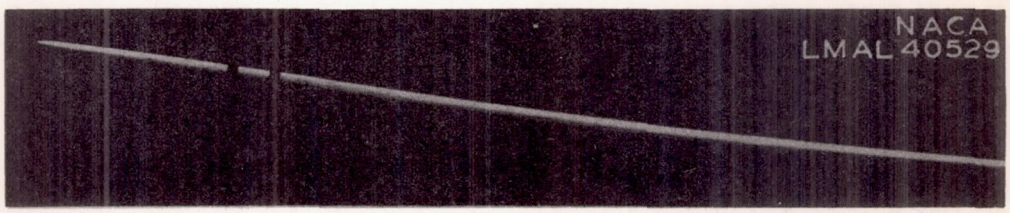

c. Condition 3.

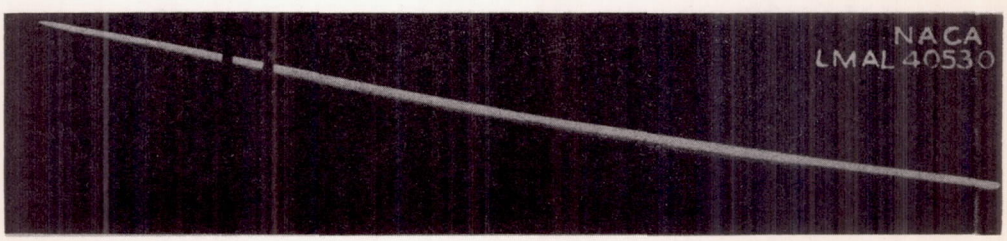

d. Condition 4.

Figure 6.- High-speed photograhs of a YR-4B production rotor blade in simulated flight conditions. Ψ, 45°.

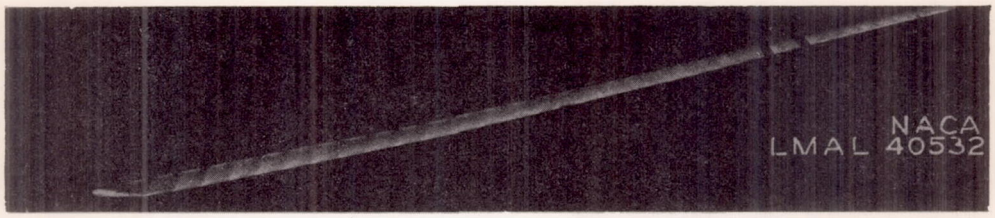

a. Condition 1.

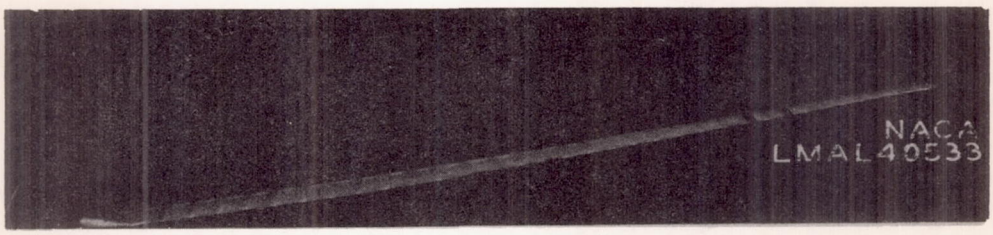

b. Condition 2.

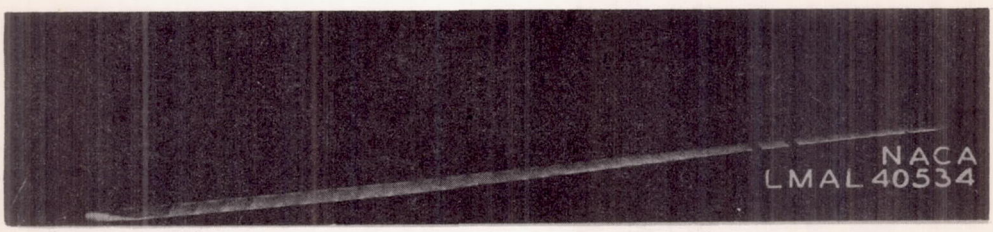

c. Condition 3.

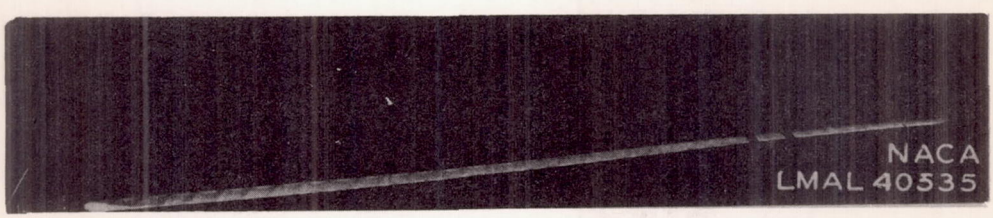

d. Condition 4.

Figure 7.- High-speed photographs of a YR-4B production rotor blade in simulated flight conditions. ψ, 135°.

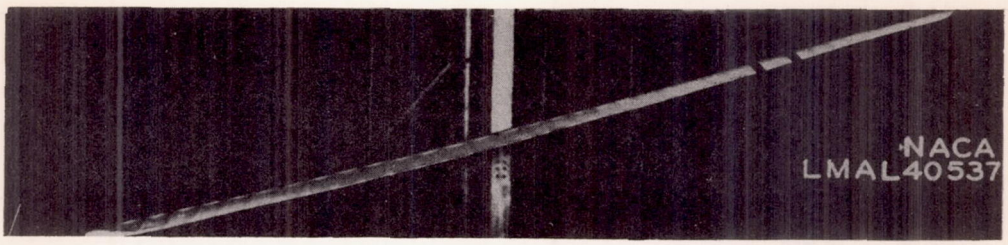

a. Condition 1.

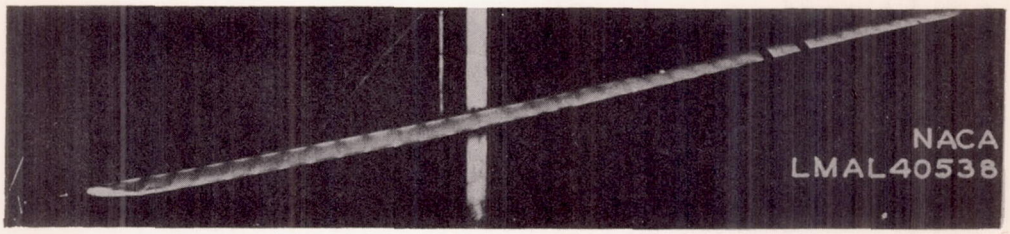

b. Condition 2.

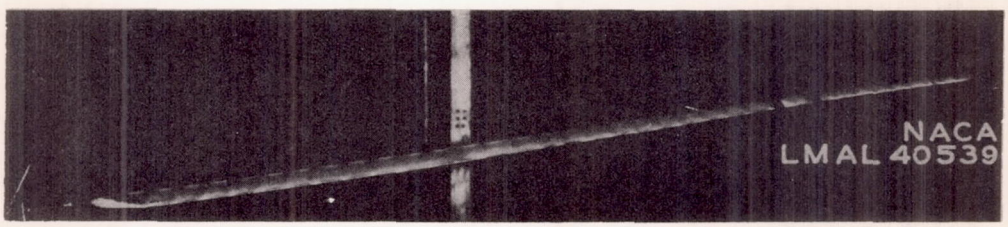

c. Condition 3.

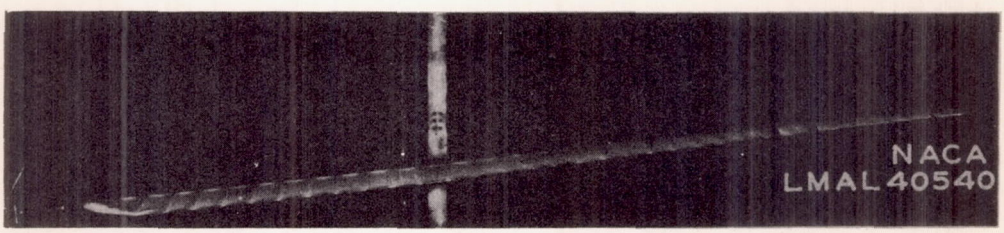

d. Condition 4.

Figure 8.- High-speed photographs of a YR-4B production rotor blade in simulated flight conditions. ψ, 180°.

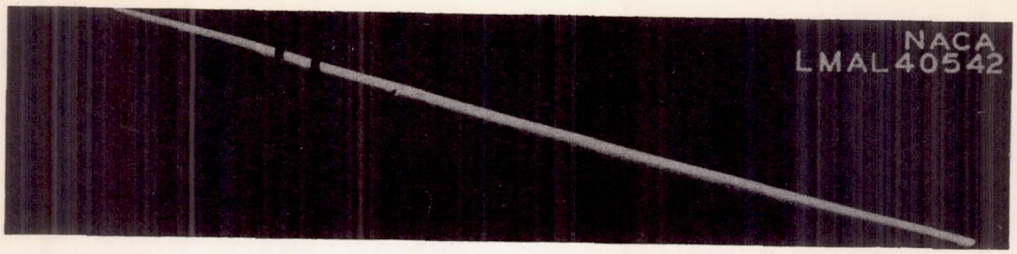

a. Condition 1.

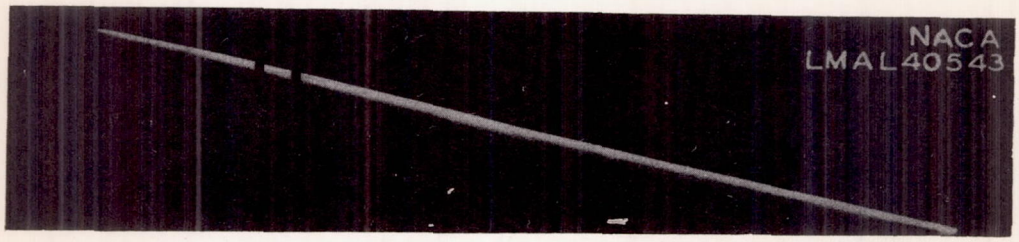

b. Condition 2.

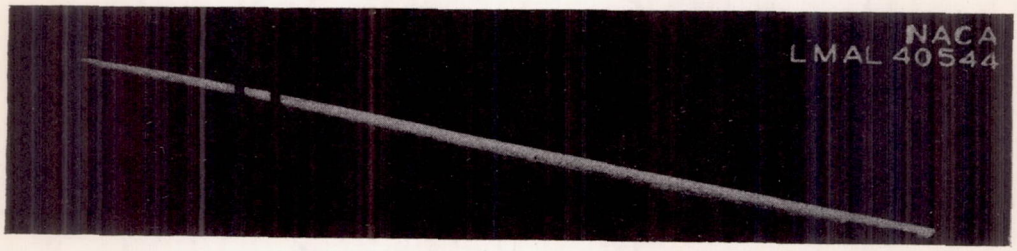

c. Condition 3.

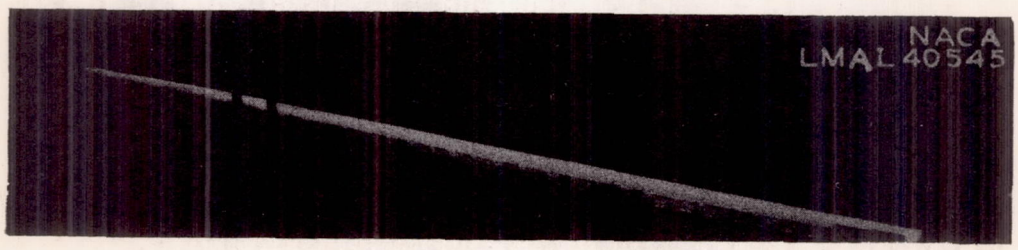

d. Condition 4.

Figure 9.- High-speed photographs of a YR-4B production rotor blade in simulated flight conditions. Ψ, 225°.

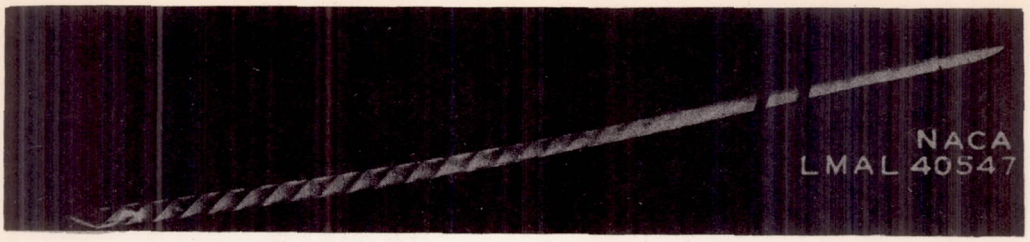

a. Condition 1.

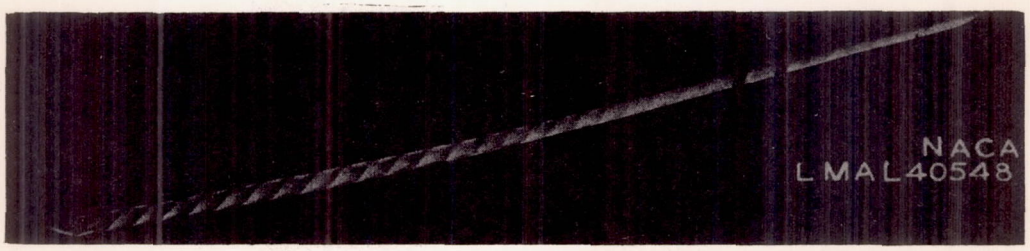

b. Condition 2.

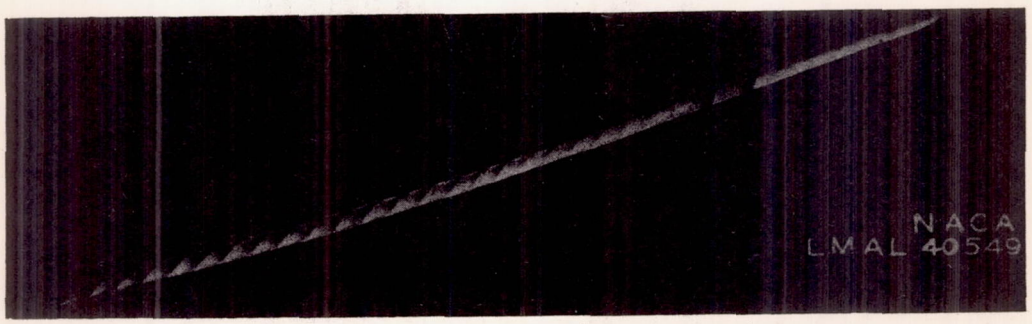

c. Condition 3.

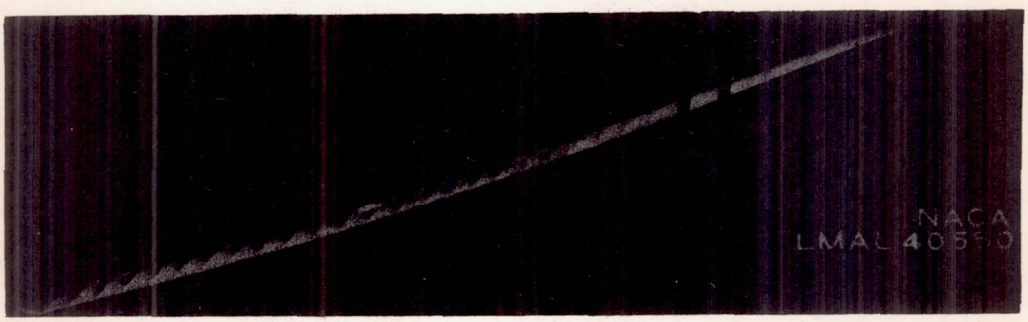

d. Condition 4.

Figure 10.- High-speed photographs of a YR-4B production rotor blade in simulated flight conditions. Ψ, 315°.

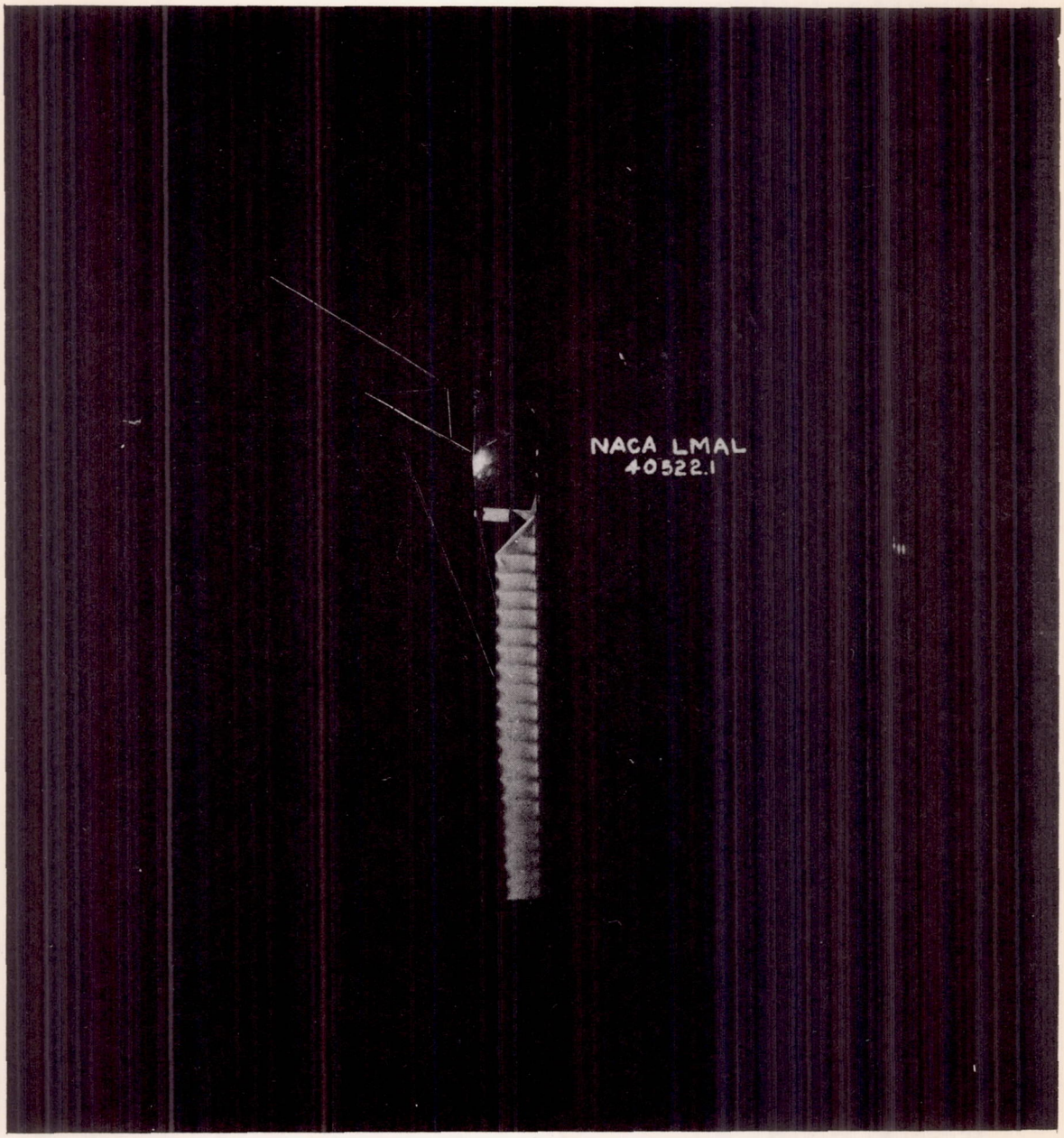

(a) Ψ, 0°.

Figure 11.- Photographs of YR-4B production blades taken with overhead camera for condition 1.

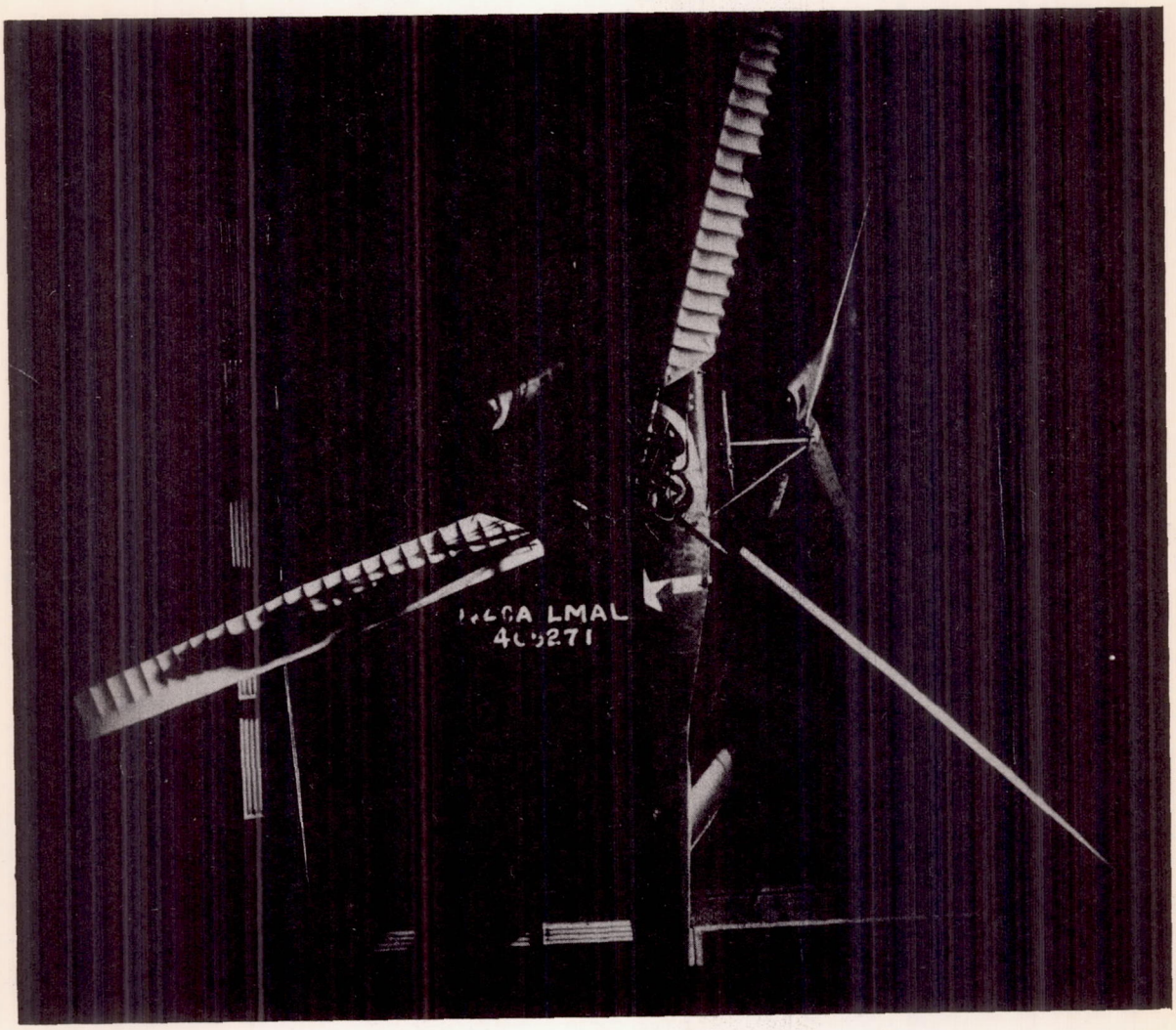

(b) Ψ, 45°.

Figure 11.- Continued.

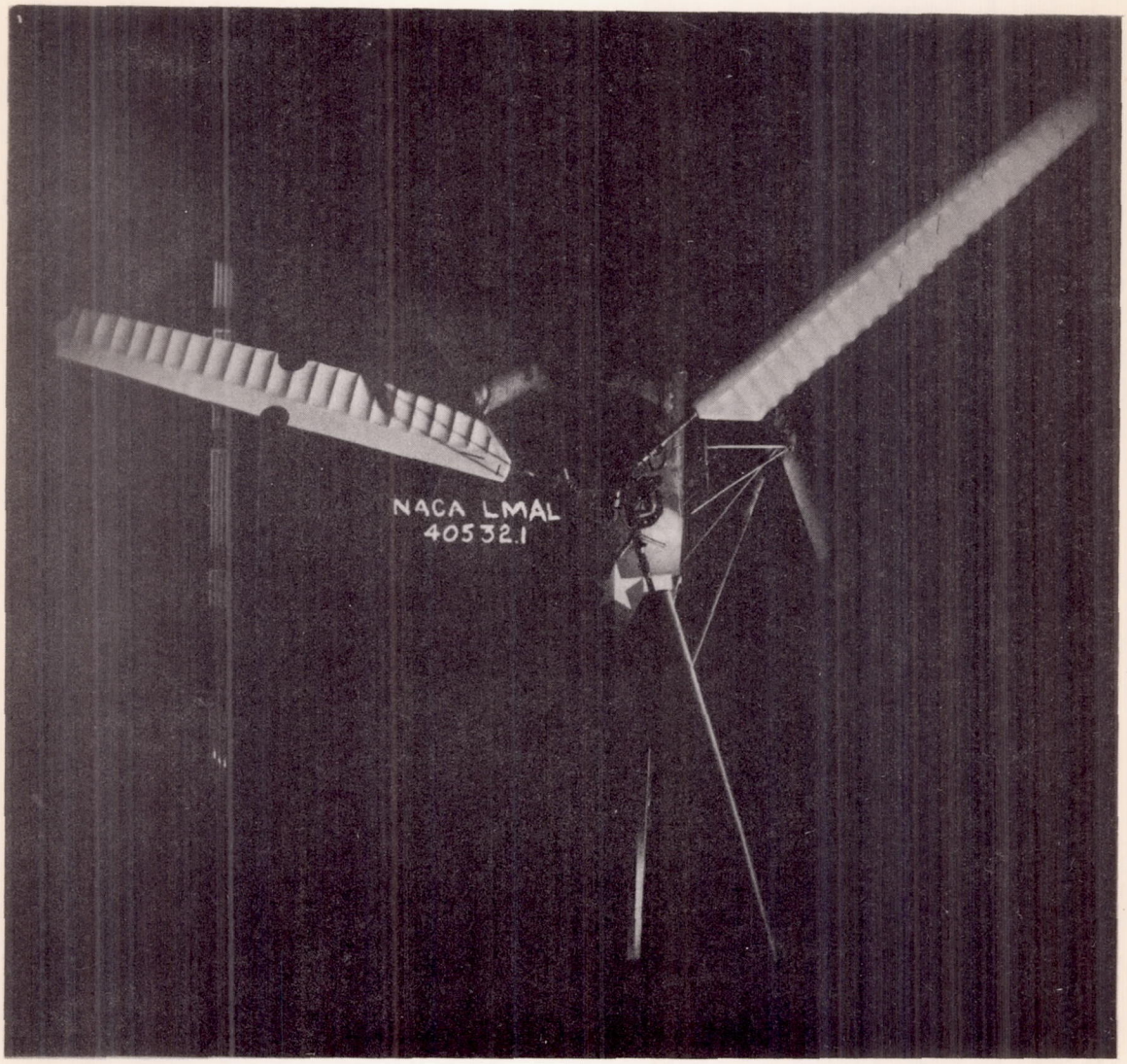

(c) Ψ, 135°.

Figure 11.- Continued.

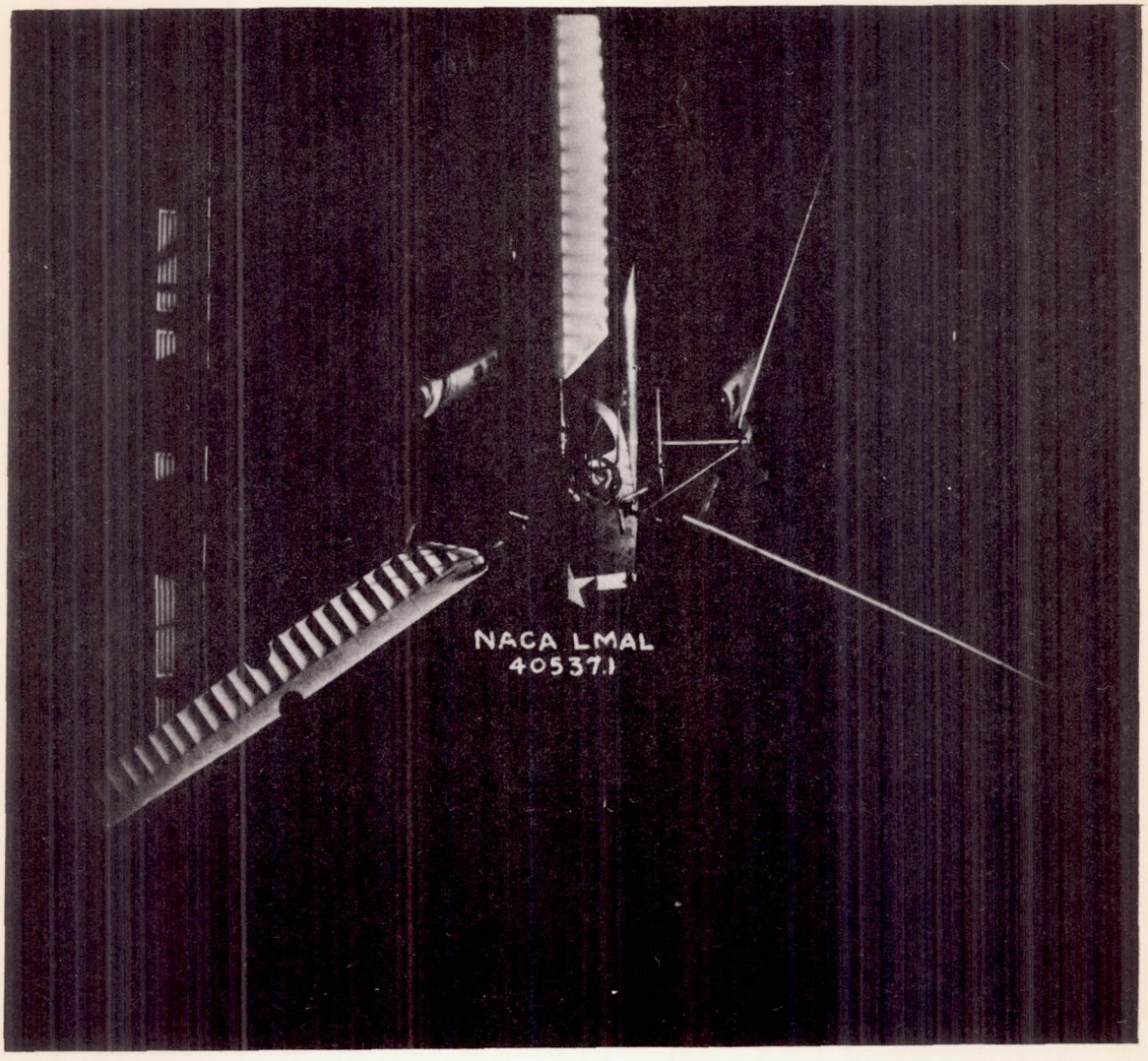

(d) Ψ, 180°.

Figure 11.- Continued.

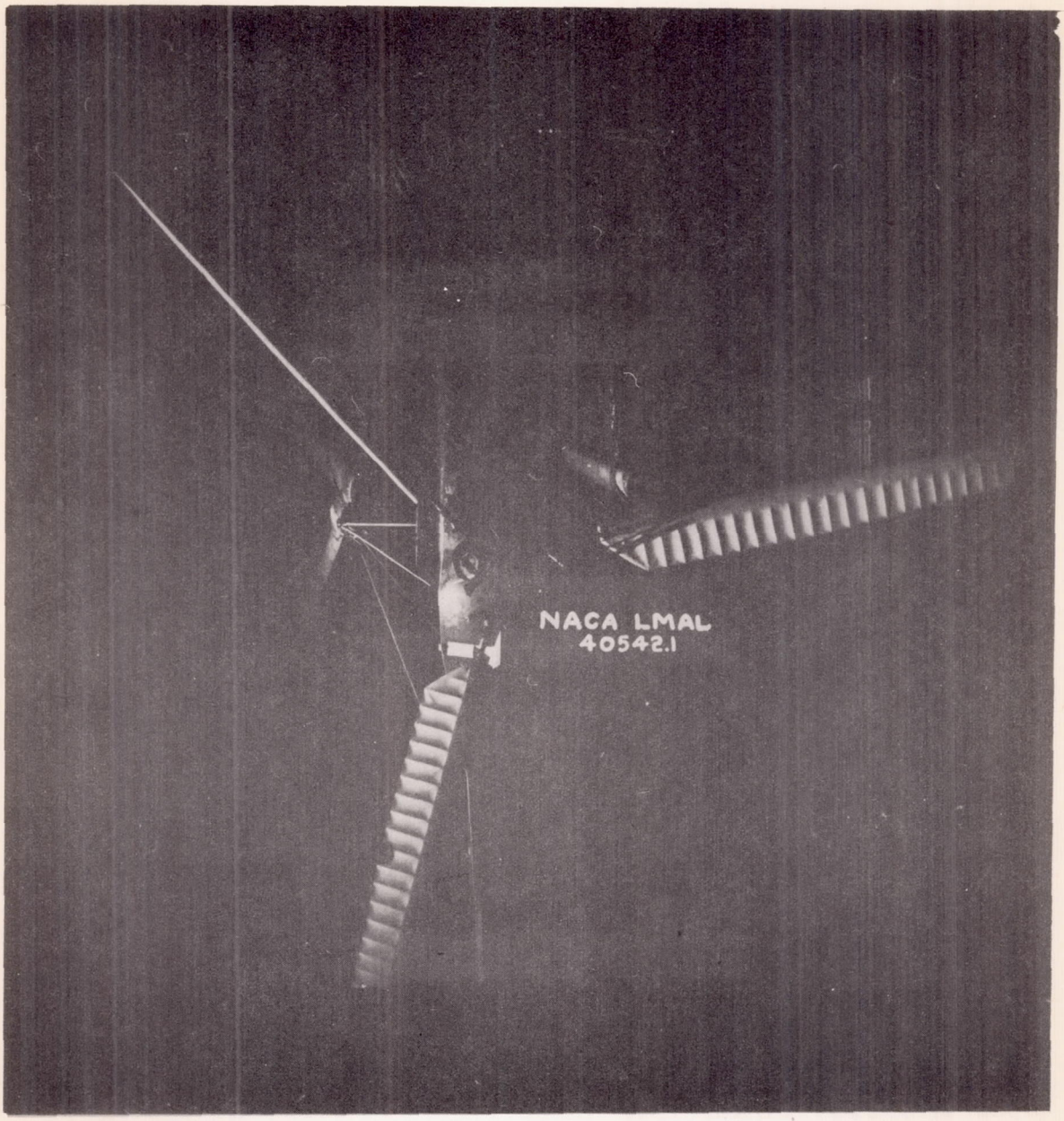

(e) Ψ, 225°.

Figure 11.- Continued.

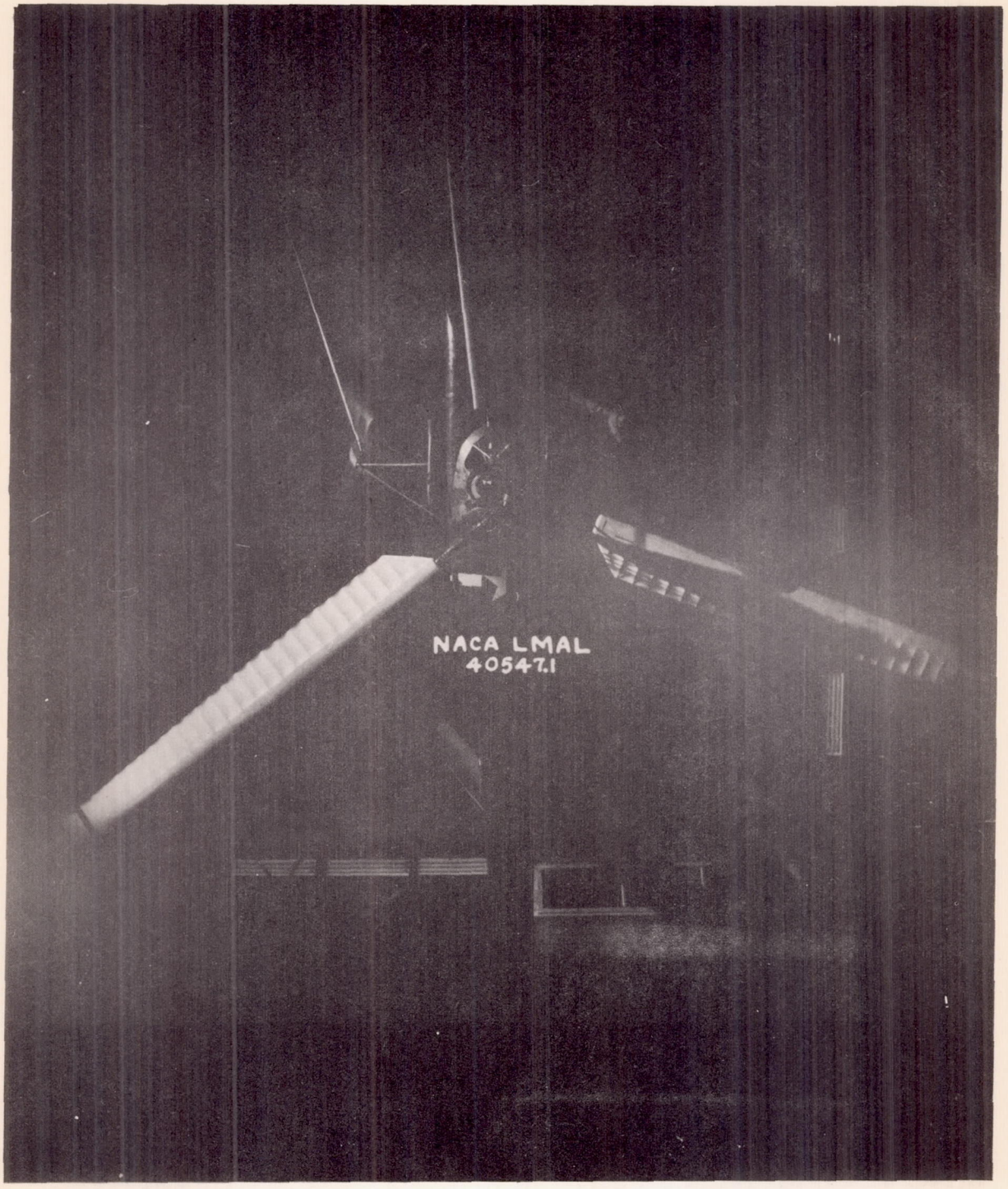

(f) Ψ, 315°.

Figure 11.- Concluded.